A SIMULATION OF HUMAN HEART FUNCTION

W. T. HANNA

From the Battelle Memorial Institute, Columbus Laboratories, Columbus, Ohio 43201

ABSTRACT A simulation of the function of the human heart and heart muscle has been developed in the form of a digital computer code. For a given set of values for the input variables, realistic values of the cardiac output variables are predicted. A detailed discussion of the simulation and some results obtained from its application are presented. This simulation represents a unique combination of what was known in muscle mechanics, muscle thermodynamics, and of the structure, size, and shape of the heart, into an engineering model to improve the understanding of human heart muscle function. The left ventricle (LV) is treated as a thick-walled sphere whose wall is composed entirely of muscle fibers. Force-length velocity relationships are used to determine the tension in each fiber. The pressure in the LV is computed from fiber tension and fiber structure in the LV. A lumped-parameter simulation of the arterial tree provides a load impedance for the LV. Results are presented for simulation of normal human LV performance.

INTRODUCTION

As evaluation of the functional state of the heart is an important problem in cases of heart dysfunction (1–3), various indices of contractility (4–6) have been devised to help quantify the functional state of the heart muscle. Many of these indices are related to basic measures of muscle performance that have been determined in experiments with strips of animal heart muscle. The development and use of these indices is an application of the knowledge gained in muscle fiber experiments, but only in a simplified manner. This simple and direct application of basic muscle mechanics has had a useful clinical result despite limitations inherent in the present indices of contractility (7–8). A better understanding of muscle function in the heart would improve the clinical usefulness of known indices and might suggest a more applicable or more discriminating set of indices of contractility.

A number of computer simulations of the hemodynamics of the human cardiovascular system have been reported (9–10). (*a*) Using analogue computers the hemodynamics of the circulatory system have been studied, i.e., the pressure and flow rate characteristics of branched networks of arteries (11–13) and capillaries and veins (14). (*b*) Other simulations have been used to study the physiological control systems that regulate cardiac output (15–18), or for teaching purposes. (*c*) The more recent simulations have considered the function of the heart in greater detail by

including some of the results of isolated heart muscle experiments (9). However, none of these simulations were developed specifically for the task of studying the function of the normal heart.

The present computer model combines the essence of the above analyses into an application-oriented engineering model to be used for studying normal and diseased heart performance under a wide variety of conditions.

NOMENCLATURE

a_l	Muscle parameter at length l.
b	Muscle parameter, length independent.
CE	Contractile element.
F_l	Fraction of cross bridges available.
F_p	Dimensionless isometric tension.
F_{SE}	Series element tension.
K_1	PE stiffness for $l > l_1$.
K_r	Relative PE stiffness for $l > l_1$.
K_{SE}	Elastic constant for SE.
K_{SV}	Viscous constant for SE.
l	Sarcomere length.
l_a, l_b	Sarcomere length at state a or b.
l_{CE}	Contractile element length.
l_0	Maximum l for $T_p = 0$.
l_s	End-systole sarcomere length.
l_{SE}	Series element length ($l - l_{CE}$).
l_1	Length at which T_p changes slope.
n	Position index.
PE	Parallel element.
P_{LV}	LV pressure.
r	Radial coordinate.
r_a, r_b	Radius at state a or b.
r_i	Inside radius of LV sphere.
r_o	Outside radius of LV sphere.
σ	True stress average over a pair of adjacent layers of fibers.
SE	Series element.
T	Total tension ($T_a + T_p$).
T_a	Active tension.
T_0	Maximum active tension.
T_p	Passive tension.
u	Contractile element velocity.
u_l	Maximum value of u at length l.
u_m	Maximum value of u at any length.
u_s	Sarcomere contractile velocity.
V	Cavity volume.
$\dot{V}$	LV outflow rate.
V_a, V_b	Cavity volume at state a or b.
V_M	Sark volume.
V_s	Cavity volume at end systole.

V_w Wall volume.
$X_{1,2}$ Axes of fiber contraction.

BASIS OF THE SIMULATION

The development of a realistic simulation of heart function requires that all the important elements of muscular function in the heart be brought into the simulation in the greatest detail possible. The primary elements considered include: (*a*) description of the shape and size of the LV, (*b*) the orientation and motion of muscle fibers in the LV wall, (*c*) the mechanics and thermodynamics of isolated muscle fiber contraction, (*d*) the hemodynamic load imposed on the LV by the systemic circulation, and (*e*) the assimilation of these four elements into a functional model. These various aspects are considered in the following sections as the basic equations governing the LV function are presented.

Description of the Shape and Size of the LV

The true shape of the LV cavity is probably best described as a thick-walled ellipsoid of revolution. However, both Burton (19) and Rushmer (20) have noted that the LV tends to become spherical during contraction. These observations tend to justify the assumption, used in the present analysis, that the LV can be simulated by a thick-walled sphere that contracts uniformly. Using data from several sources, Beneken and DeWit (9) determined an average ratio of LV wall thickness to LV inside radius of 0.36 at the end of diastole, i.e., the normal maximum LV volume after filling was completed. In this simulation, assuming that the LV wall is incompressible and that all the muscle fibers in the wall are incompressible leads to the result that the LV wall thickness increases during LV contraction. The radius to some point in the LV wall can be given in terms of an index n which specifies the fraction of the volume of the wall contained in the sphere of radius r:

$$r = [0.75\ (V + nV_w)/\pi]^{0.33}. \tag{1}$$

According to Burton (19) a normal, healthy male, 30 yr old, might have an end diastolic volume (EDV) of 150 cm^3 and would eject 75 cm^3 of blood per beat (stroke volume or SV). The LV wall volume (using data from reference 9) would be approximately 225 cm^3 for such a person.

Muscle Fiber Structure and Muscle Mechanics

A section of skeletal or cardiac muscle is composed of an array of single-cell muscle fibers where each fiber is approximately 80 μm long and 10–15 μm in diameter. The fiber contains contractile structures called sarcomeres, which are the ultrastructural unit of the muscle. The sarcomere is the shortest structure in the fiber which changes

length during muscle contraction; in skeletal muscle the sarcomere length varies between 1.5 and 3.6 μm, in cardiac muscle the length range is 1.5–2.5 μm.

A basic contractile unit, here called a "sark" to distinguish it from muscle filaments which are called myofilaments, is defined as a thick myosin filament and the six thin actin filaments surrounding each end of the myosin. A sark has the shape of a hexagonal prism, as shown in Fig. 1, and is assumed to have constant volume; hence, its cross-sectional area increases during contraction.

Several investigators who have studied the contraction of muscle include Hill (21) and Huxley (22), who primarily studied the mechanics of muscle contraction. Using the methods of irreversible thermodynamics, Caplan (23), Wilkie and Woledge (24), and Bornhorst and Minardi (25) studied not only the mechanics but also the energy conversion processes in muscle. In 1970, Bornhorst and Minardi (26, 27) developed a phenomenological theory of muscular contraction and applied it to skeletal muscle experimental data. An important result of this theory is a set of phenomenological equations which describe the force-length-velocity relationship between force and the rate of the chemical reaction driving the contraction. Other researchers have developed theories of muscle contraction which can be incorporated in the present analytic model after development in sufficient detail. However, because of its completeness and favorable comparison with experimental data, the Bornhorst and Minardi theory is used to describe the phenomenology of muscle contraction in this

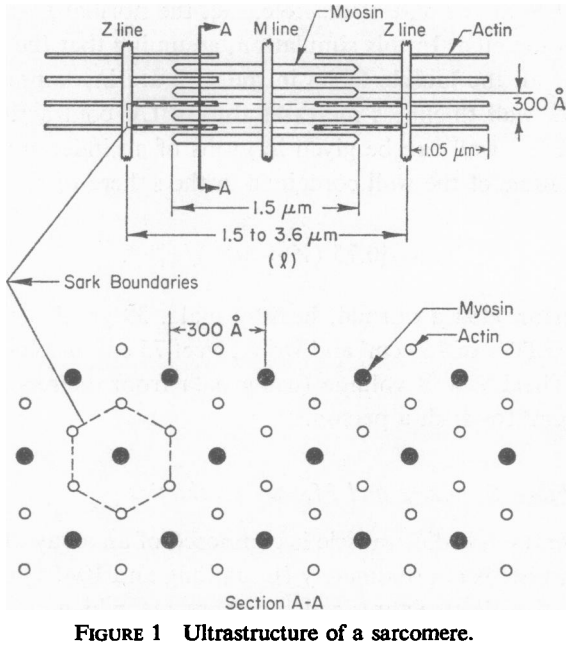

FIGURE 1 Ultrastructure of a sarcomere.

heart simulation. A detailed development of the theory is given in references 26 and 27, but a review of the results applicable to the heart simulation are given here.

The primary result is a form of Hill's (22) equation relating force T_a to contractile velocity u by:

$$T_a = a_l(u_l - u)/(b + u), \tag{2}$$

where a_l and b are parameters having the units of force and velocity, respectively, and u_l is the maximum velocity of contraction at any sarcomere length l. Eq. 2 is essentially Eq. 20 of Bornhorst and Minardi's development (27). The parameters a_l and u_l are defined in terms of two dimensionless functions of length F_l and F_p.

$$a_l/T_0 = F_l\,(l + b/u_m) - F_p\,, \tag{3}$$

$$u_l/u_m = F_p b/[u_m(a_l/T_0)]. \tag{4}$$

The number of cross bridges available for activation for a given sarcomere length is given by F_l as deduced from the structure of the sarcomere. The function F_p is the ratio of isometric (static) force developed at length l to the maximum isometric force developed at sarcomere length l_0. The variation of F_l and F_p with sarcomere length for skeletal muscle is shown in Fig. 2 along with the curves showing a_l/T_0 and u_l/u_m as functions of sarcomere length, where T_0 is the maximum isometric force and u_m is the maximum contractile velocity. The combination of Eqs. 2–4, using the functions F_l and F_p, gives a description of the dynamics of contraction of a representative sarcomere in the heart. This description is the most important aspect of the entire heart model since it governs the contraction of all the sarcomeres

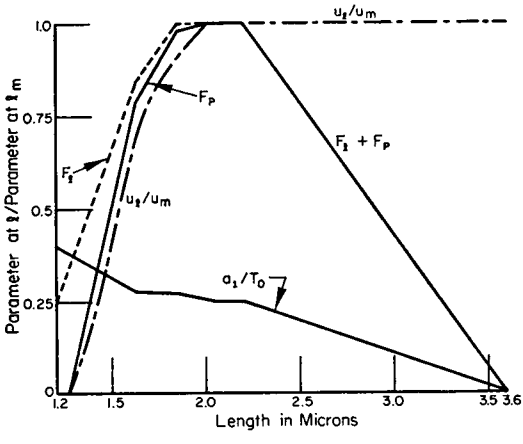

FIGURE 2

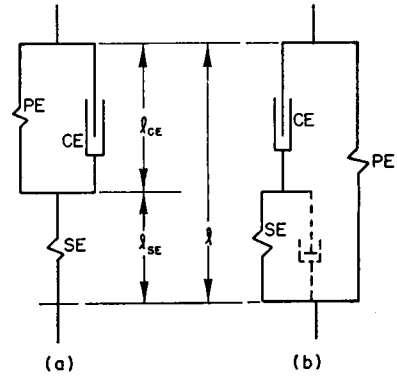

FIGURE 3

FIGURE 2 Muscle parameters as a function of sarcomere length.
FIGURE 3 Conceptual components of muscle fibers, (*a*) Voigt, (*b*) Maxwell, with viscoelastic series element.

of the model. This description applies only to fully stimulated myofilaments and the transition from an unstimulated to a fully stimulated condition is accommodated by a stimulation factor discussed later. The experimental data used in determining the functions shown in Fig. 2 are basically those of Gordon et al. (28) for frog skeletal muscle. Although the use of skeletal muscle data introduces some limitation on the results of the heart model, the differences between skeletal and cardiac muscle are slight. The value of the parameter b is 0.25 u_m, so that at $l = l_0$, $a_l/T_0 = b/u_m$ and Eq. 2 becomes the familiar Hill equation.

Experiments on isolated animal muscle fibers have shown that the contractile dynamics of the fiber cannot be adequately described solely by force-length-velocity relationships as described above. These relationships do not consider the elasticity of the fiber which appears to be quite important. Two approaches have been developed to combine the elastic and contractile aspects of muscle using conceptual mechanical analogies of the muscle fiber. These two analogies, known as the Voigt[1] and Maxwell "models" (29) are two different arrangements of elastic elements around a contractile element (CE) as shown in Fig. 3. The CE is freely extensible when unstimulated and is governed by force-length-velocity relationships, such as those discussed above, when stimulated. The series element (SE) and parallel element (PE) are nonlinear springs, always in tension, simulating the elasticity of a muscle fiber. The dashpot shown adjacent to the SE in the Maxwell model (Fig. 3 *b*) represents the viscous behavior of the muscle fiber. The question of which model, "Voigt" or "Maxwell," is the most realistic has been the subject of much research. A recent study by Fung (30) has shown that these two models are equivalent, although the Maxwell model is preferred due to its simpler mathematical formulation, hence, a modified form (viscous SE) of the Maxwell model is employed here. The PE represents a nonlinear elasticity which may reside in the membranes surrounding the muscle fiber, or fibrils, and thus is not inside the sarcomere. In this model the PE is characterized by the following relation between the passive, or resting, tension T_p acting on a sark and the sarcomere length l:

$$\begin{aligned} T_p &= 0, \quad \text{for} \quad l \leq l_0, \\ T_p &= K_1(l - l_0), \quad \text{for} \quad l_0 \leq l \leq l_1, \\ T_p &= K_1[(l_1 - l_0) + K_r(l - l_1)], \quad \text{for} \quad l > l_1. \end{aligned} \tag{5}$$

The specific values used for K_1, K_r, l_0, and l_1 were selected to give a good approximation of both the passive-length tension curves for animal papillary muscle and the pressure-volume curves for the intact animal LV (31, 32). The SE represents muscle fiber elasticity that may reside in the chains of protein molecules in the sarcomere or in the tissue connecting fibrils and fibers. The SE is characterized by a

[1] It should be noted that despite the names "Maxwell" and "Voigt" these models are not viscoelastic and are not related to the models for viscoelastic solids and fluids which have the same names, respectively.

linear viscoelastic element in this simulation. The presence of viscous effects in muscle tissue has not yet been measured experimentally, but, in view of the fact that muscle cells contain considerable quantities of liquid, the presence of viscous effects in muscle fibers must be accounted for in the analysis.

The CE has two states, diastole and systole, which are the relaxed and the active states, respectively. In diastole the CE is assumed to be freely extensible, exerting no force on the SE. When fully activated in systole the CE force-velocity relationship is given by the phenomenological theory of muscle contraction discussed previously. The force and velocity of the CE are the variables T_a and u in the modified Hill's equation (Eq. 2 above). The CE length (l_{CE}) is used to determine the values of F_p, a_l, and u_l used in the Hill equation. As shown in Fig. 3 *b*, l_{CE} plus the SE length l_{SE} make up the sarcomere length l. The transitions between diastole and systole are accomplished by linearly increasing or decreasing the value of T_0, the maximum contractile force. T_0 is zero during diastole; after transition it has a constant value during systole and then is decreased to zero for the next diastole. The duration of the two transition periods in each heart cycle is inferred from data taken showing the rate of rise of tension in isometric muscle experiments. The dimensionless ratio of the instantaneous value of T_0 to its maximum value is defined as the stimulation factor. The total tension T carried by a basic contractile unit is the sum of the active and passive tension:

$$T = T_a + T_p. \tag{6}$$

LV Structure and Fiber Orientation

A thick-walled spherical shape has been assumed for the LV in this simulation. The spherical shape is maintained during the heart cycle, hence, the sphere must contract uniformly. This implies that at any radial position in the wall the stresses in a tangent plane are the same in any direction in the plane, thus requiring that the stresses are the same in any two orthogonal directions. Since muscle fibers can only support tension in their axial direction, a spherical ventricle must have equal numbers of muscle fibers in two orthogonal directions at any location on the spherical surface. This is achieved by assuming that the muscle fibers are arranged in pairs of layers, with the fibers in adjacent layers being mutually perpendicular as shown in Fig. 4. This assumed fiber orientation does not conform well with the experimental observations of Streeter (33, 34) and is not uniformly applicable to the entire sphere. It does, however, approximate the earlier views of fiber orientation in the heart wall (20) and provides a simplistic view allowing a highly simplified analytic approach. Since the thickness of each layer is one fiber diameter, the ratio of layer thickness to the radius of curvature of the layer is very small, $\approx$0.001, and the curvature of adjacent layers is nearly the same. This result is mathematically convenient in relating fiber tension to LV pressure.

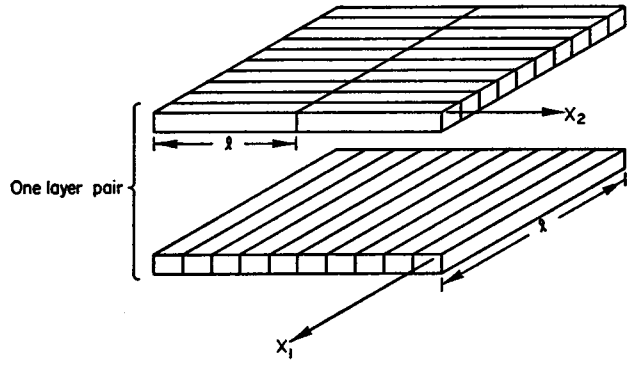

FIGURE 4 Fiber orientation in a pair of adjacent layers. The axes X_1 and X_2 are perpendicular axes of fiber contraction.

LV Pressure and Volume

Using the fiber orientation defined above, the effective stress acting along the axis of either layer of fibers of a pair of layers is given by

$$\sigma = Tl/2V_M . \tag{7}$$

Division by a factor of 2 results from consideration of pairs of orthogonal layers as indicated in Fig. 4. The pressure in the LV can be related to the muscle stress by requiring that any hemisphere of the heart wall is in a state of dynamic equilibrium with LV pressure balancing muscle stress. The equilibrium relation is expressed by

$$P_{LV}(\pi r_i^2) = 2\pi \int_{r_i}^{r_o} \sigma r dr. \tag{8}$$

The stress is not a simple function of radial position, since it depends upon sarcomere length and contractile velocity; hence, the integration in Eq. 8 must be done numerically. This integration is facilitated by expressing the stress and radial position in terms of LV volume and outflow rate and an index specifying radial position in the LV wall. The relationship between σ and (V, $\dot{V}$, and n) is developed by first relating sarcomere length to V and n. Assume that the layers of muscle fibers form thin spherical shells with continual contact between adjacent layers, and further that the fibers and the sarcomeres do not buckle as the heart contracts. With these assumptions a change in LV cavity volume will result in a sarcomere length change which is proportional to the change in radius of the sarcomere. That is,

$$l_a/l_b = r_a/r_b , \tag{9}$$

where subscripts a and b refer to two different LV cavity volumes V_a and V_b. The radius of curvature of a sarcomere is a function of both the cavity volume and the

sarcomere's position in the wall. In writing Eq. 9 only the cavity volume changes between states a and b, the wall position index n is not changed, hence, the same sarcomere is considered in each state. Sarcomere lengths in the heart have been measured by Spotnitz (32) at various volumes between the EDV and the end systolic volume (ESV). A reasonable representation of these data may be given by

$$l_s = 1.55 + 0.1n \quad \text{(microns)}, \tag{10}$$

where l_s is the sarcomere length at end systole. By combining Eqs. 1, 9, and 10 the sarcomere length at any cavity volume and radial position is expressed by

$$l = (1.55 + 0.1n)[(V + nV_w)/(V_s + nV_w)]^{0.33}. \tag{11}$$

By differentiating Eq. 11 with respect to time, a relationship between the sarcomere contraction velocity and cavity volume is obtained. With the definitions

$$u_s = -\,\mathrm{d}l/\mathrm{d}t \quad \text{and} \quad \dot{V} = -\mathrm{d}V/\mathrm{d}t, \qquad \text{there results } u_s = \dot{V}l/3(V + nV_w). \tag{12}$$

Assuming that the inertia of the muscle fiber is negligibly small, a force balance on the CE and SE shows that the tension developed in the CE is equal to the force supported by the SE;

$$T_a = F_{SE}, \tag{13}$$

$$T_a = T_0(a_l/T_0)(u_l - u)/(b + u), \tag{14}$$

$$F_{SE} = K_{SE}(l - l_{CE}) + K_{SV}(u - u_s). \tag{15}$$

Eqs. 13–15 can be solved for u in terms of l, u_s, u_l, T_0, and a_l/T_0 which are known, and l_{CE}, which is unknown. However, l_{CE} can be obtained by integrating u from the initiation of a contraction when $u = u_s = 0$ and $l_{CE} = l$. Once u_s is obtained, Eq. 14 gives T_a and σ may then be evaluated.

The LV pressure can be written in terms of the variables V and $\dot{V}$ providing that the stress is integrated over the LV wall, from $n = 0$ to $n = 1$. The integration is performed by dividing the LV wall into 10 spherical shells of equal volume and evaluating the stress at each shell boundary. The integral is the summation of the average shell stress acting over the total cross-sectional area of each shell.

Aortic Hemodynamics

This simulation of the LV has resulted in one equation relating two variables: pressure and flow rate. A second equation relating these variables is needed before the solution is mathematically complete. This other relation is derived by considering the load imposed on the LV by the systemic circulation. Simulations of the hemodynamics of the arterial and venous systems have been developed by Noordergraaf

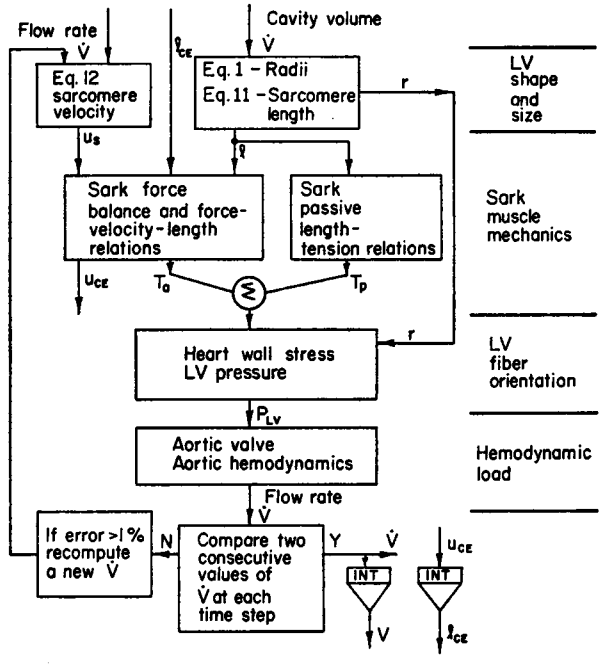

FIGURE 5 Flow chart of computation in program.

(10), Jager et al. (11), Beneken and DeWit (9), Dick and Rideout (13), Snyder and Rideout (14), and Snyder et al. (12), among others. The above simulations were implemented on analogue computers, but any of them could be reprogrammed for a digital computer. The simulation reported by Snyder et al. (12) was used in most of the present actual simulation computations, although with somewhat different values for the various aortic parameters than reported by Snyder.

Model Synthesis

The synthesis of the functional heart model from the basic elements is perhaps the most important aspect of the model. The flow chart, Fig. 5, shows the way in which the four basic elements of the heart model are combined to compute the required intermediate and output variables. The program begins at an initial condition at which LV outflow rate and cavity volume are known. These variables, combined with the assumptions about LV shape, size, and structure, and with Eqs. 1, 11, and 12, give values for LV wall radii and sarcomere length and velocity. These variables, along with the CE length are combined with the basic muscle mechanics relationships to predict the active and passive sark tension. This step brings in the length-dependent Hill equation (force-velocity relationship) and the stimulation factor. The next step in the flow chart is the evaluation of the average fiber stress and its integration over the thickness of the heart wall to give the LV pressure. These cal-

culations are based upon the instantaneous size of the LV (radius) and the fiber orientation. Finally, the aortic simulation is used to determine a new value of LV outflow rate, given the value of LV pressure and the pressures and flow rates at various points down the length of the simulated aorta.

Computation

The basic computation is done using a time-stepping technique. The LV and aortic simulations are initialized to the end diastolic condition, then at each successive time step the pressure and flow rates are evaluated throughout the aorta, using the most recently computed values available for each variable. Then, using the most recent values for LV outflow rate and LV cavity volume, LV pressure and aortic pressure are reevaluated. A new value of outflow rate is computed using the new V and aortic pressures. This calculation uses an approximate pressure-drop vs. flow rate characteristic for the aortic valve. The calculation of LV pressure and outflow rate is then repeated until successive values of outflow rate are within 1%. This iteration process assures that the LV simulation gives flow rate and pressures which are consistent with the contractile state. At this point, time is incremented and all aortic calculations are repeated with the new value of outflow rate. This process is continued until the end systolic condition is reached and the cycle is then completed.

Summary of Model

A brief review of the inputs required and the outputs computed by the model is in order. The LV model requires the size of the heart in terms of the normal maximum and minimum cavity volumes and the volume of muscle in the heart wall. The sarcomere length at some stage of contraction is also required. Here, data at end systole are generally used. The basic muscle parameters required are the length-tension-velocity relationship for the CE and the SE and PE properties. The PE length-tension curve is taken from passive muscle experiments. Experiments with papillary muscle have also indicated the SE length-tension properties, the SE extension being about 5% (29) of the initial muscle length at maximum tension. The viscous properties of the SE have not yet been experimentally measured; however, some damping is known to be required for stability in the simulation of the muscle fiber dynamics. The value of the viscous constant was chosen so that the SE could relax in 10 ms, which is fast relative to contraction times, and thus is not in conflict with experimental results. The time-course of the stimulation factor is shown on the bottom of Fig. 6; the stimulation factor is the ratio of the maximum isometric tension at any time to the true maximum isometric tension. The length of the period of stimulation is the same as the experimental systolic period, and the duration of the transitions was determined empirically by optimizing the correlation between computed and experimental LV pressure. Similarly, the values for elasticity, fluid inertia, and viscous flow resistance of the aortic segments were adjusted to give the best possible

correlation between computed and experimental values for LV pressure, aortic pressure, and LV flow rate.

The computed results of the model fall into two types: (*a*) values for those variables which are measurable and can be compared with experimental results and, thus, are used to establish the validity of the simulation; and (*b*) values for those variables for which no experimental data exist for comparison and are predictive in nature. The comparative variables are the pressures in the LV and aorta, and the outflow rate and volume of the LV. The predictive variables include the sarcomere length, the CE length, the contractile velocity of the sarcomere and the CE, the average tangential stress in the LV wall, and the CE power developed. All of these variables are evaluated for each of the 10 shells in the LV wall at 10 ms intervals. This is the first analysis of the dynamics of the human LV which predicts these variables during contraction. Since the comparative variable values (pressure and flow rate) are computed from the more basic predicted variables, the predicted variables are, in a real sense, calibrated by requiring the pressures and flow rate to match experimental data. Thus, the model can be used to gain a detailed view of the contractile state of the muscle of a specific heart, with some degree of confidence in the predicted results.

RESULTS FROM THE SIMULATION OF EXPERIMENTAL DATA

The results presented here were selected to show the capability of the model for realistic simulation of LV function. The comparative results of this model are presented in Figs. 6 and 7, along with experimental data of Burns and Griffith (35). A comparison of the computed and experimental results presented in these figures indicates that a remarkably good simulation of the human heart has been obtained. The predicted LV pressure does not have the more gradual initial rise and final decay of the measured pressure. This is very likely due to the fact that in the model the LV is stimulated uniformly as a function of time, where in vivo there is a wave of stimulation which travels through the LV wall at a finite velocity. However, this is the rate compensated for by the fact that the rate of rise of computed LV pressure is not as great as the rate of rise of the measured LV pressure. This appears to be a result of assuming that the SE is a *linear* viscoelastic element, when experimental measurements indicate that the SE stiffness actually increases with load (29, 30). A computation made with a slightly stiffer SE (increased force at comparable extension) resulted in less satisfactory results, but the rate of rise of the computed pressure increased. The aortic pressure as computed and as experimentally measured is also shown in Fig. 6. The lag in the rise of the computed aortic pressure relative to the experimentally measured curve is due to both (*a*) the lower rate of rise of computed LV pressure, and (*b*) a small lag into all the aortic pressures and flow rates introduced the numerical integration scheme used in the computer program. There

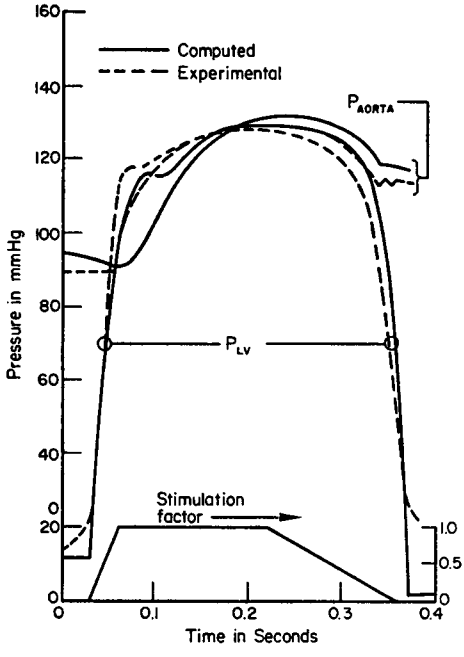

FIGURE 6

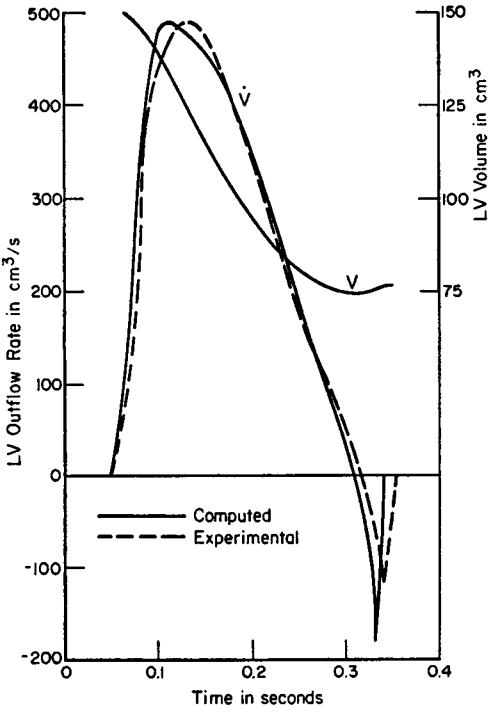

FIGURE 7

FIGURE 6 LV and aortic pressure from experimental data and computer simulation. Dimensionless stimulation factor is also shown.

FIGURE 7 Outflow rate and volume from computer simulation and experimental outflow rate.

is evidence of a dicrotic notch in the computed aortic pressure curve; however, the time scale of this effect is short relative to the basic time scale of the program and thus, the multiple oscillations of the experimental pressure curve are not seen in the computed curve.

The computed and measured flow rates are shown in Fig. 7 along with the computed LV cavity volume for the model. The negative flow rate at end systole is due to a small amount of aortic regurgitation or perhaps bulging of the aortic valve leaflets as the LV pressure decreases. This backflow was induced in the model by a time delay in aortic valve closure, simulating the dynamics of an actual valve.

The time variation of the LV pressure, aortic pressure, and aortic flow rate predicted by Beneken and DeWit's analogue simulation are shown in Fig. 8. These have been redrawn from oscilloscope tracings (9) and may include minor inaccuracies. These results are presented to show the improved capability of the present model relative to this early model. The comparison of the results of the two models is presented because of their similarity, i.e., both are thick-walled special models of the LV and both consider to an extent the mechanics of muscle fibers. The com-

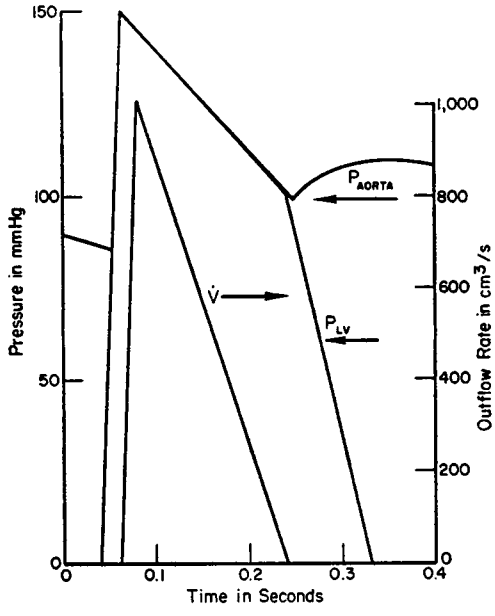

FIGURE 8

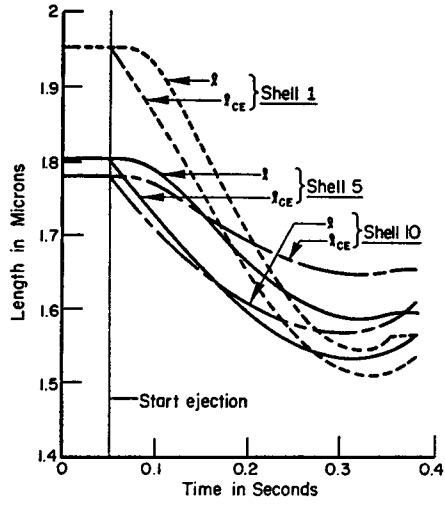

FIGURE 9

FIGURE 8 LV outflow rate, LV pressure, and aortic pressure from simulation by Beneken and DeWit (9).

FIGURE 9 Sarcomere length and CE length as functions of time at endocardium, midwall, and epicardium.

parison is interesting, but should not be carried too far since the parametric description of the heart that the earlier model was simulating is not available. It is believed that the present model yields physiologically realistic results for a normal human, as shown by several authors (19, 20, 36).

The predictive results of the model are shown in Figs. 9–12. These results are all presented as functions of time, and for various shells in the LV wall, showing both time and position variations of each variable. The sarcomere length and CE length are shown in Fig. 9 for shells 1 (inside wall or endocardium), 5 (midwall), and 10 (outside wall or epicardium).

The sarcomere length distribution at the ESV is that reported by Spotnitz (32) and incorporated into the model in Eq. 10. The sarcomere length at any other volume is the result of length changes and the spherical geometry of the model. The extremely short CE length at end systole leads to low active tension, but none of the CEs are so short that they cannot develop some tension.

The contractile velocity of the sarcomeres and CEs in shells 1, 5, and 10 are shown in Fig. 10. The rapid changes in CE velocity early in the contraction are difficult to detect in the CE length curves, despite the fact that the CE length is obtained by integrating the velocity. This clearly illustrates the difficulty in calculating VE velocity from experimentally measured length changes in isolated muscle fibers.

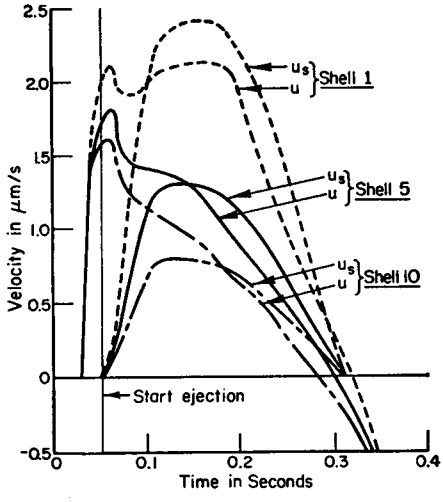

FIGURE 10 Sarcomere velocity and CE velocity as a function of time at endocardium, and epicardium.

The peak value of CE velocity occurs early in the contraction, but this peak velocity is not more than one-half of the theoretical maximum contractile velocity of an unloaded muscle fiber at the same length. Thus, an index of contractility which measures the peak CE velocity before the ejection of blood from the LV would not give an accurate value of the true maximum CE velocity u_m. The measurement may well be an index, related to u_m, and may have clinical usefulness, but it does not represent an accurate estimate of u_m in this case.

A related point concerns the use of "static" models of stresses in the LV wall. Such models have been used to estimate the LV stresses just before ejection, when the LV pressure is fairly high, but there is no outflow. The computed values of CE velocity show that the CE is not in a static situation just before ejection. This does not necessarily invalidate the stresses computed by a static model. It does imply, however, that the maximum isometric stress estimated by such models is lower than that which the fibers can actually develop.

The average shell stress is shown in Fig. 11 for shells 1, 5, and 10. The maximum stress on the order of 2 g/mm^2 agrees well with stress in static models (37). The time-course of the stress in the outermost shell (shell 10) follows the LV pressure variation, but this is not the case for the inner shells. This is the result of the LV geometry and sarcomere length distribution. The inner shells have a greater length change than outer shells, and since the length changes occur in the same time interval, the velocity is higher for fibers on the inside of the wall than those on the outside. Thus, the inner fibers operate at a relatively lower force. This is partially offset early in the cycle because the inner fibers are initially longer and, hence, can develop higher forces than the outer fibers. Later in systole, however, the CE lengths are

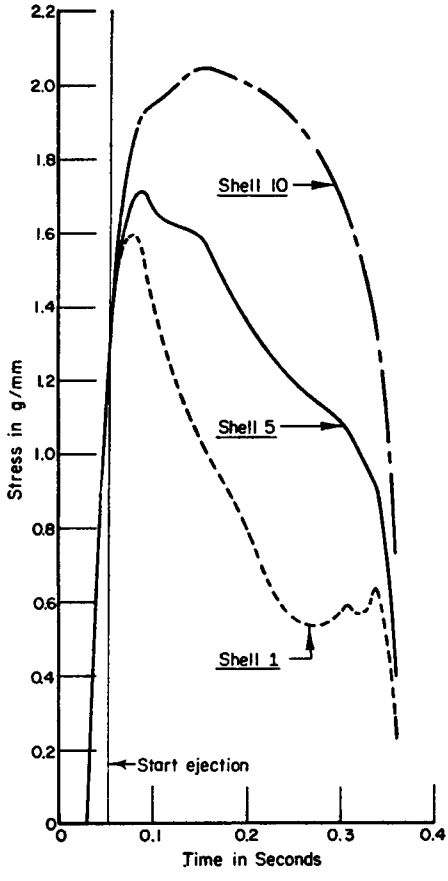

FIGURE 11

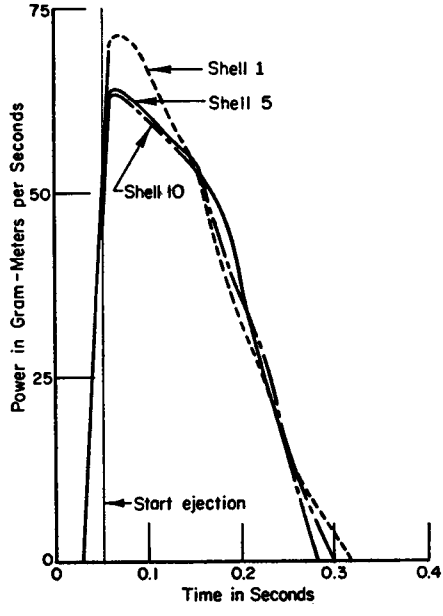

FIGURE 12

FIGURE 11 Average stress as a function of time at three locations.
FIGURE 12 Shell power as a function of time.

TABLE I

KEY HEART MODEL PARAMETERS

Maximum contractile stress	16.5 g/mm^2
Optimum sarcomere length	2.2 μm
Passive muscle stress (at optimum length)	1.5 g/mm^2
LV wall muscle volume	225 cm^3
LV EDV	150 cm^3
LV SV	75 cm^3
Heart rate	72 min^{-1}
Systolic duration	0.38 s
SE elastic constant	92 g/mm^2 per μm
SE viscous constant	1.8 g/mm^2 per (μm/s)
Myofilament maximum contractile velocity	4.8 μm/s

more nearly the same and, with their high velocity, the inner fibers develop less force than the outer fibers.

The power developed by the CEs in a shell is presented in Fig. 12 for shells 1, 5, and 10. These curves show that despite large shell-to-shell differences in stress and CE velocity, the shells develop nearly the same power. This indicates that CE power per shell may be a useful index of contractility since, in the normal heart, it is independent of LV geometry. Further studies are, of course, needed to establish the limitations and usefulness of such an index. At this time, it can only be computed using an analytic model of the LV such as the present one. The use of total LV power as an index of performance has been suggested previously (38) as being a potentially more sensitive index of performance than other hemodynamic indices. The evaluation of CE power per unit volume at any location in the heart wall may well yield more detailed information on muscular performance than total power, but its relevance and relation to reality will depend on the level of detail incorporated into the mathematical description.

A list of the primary input data for the model and their numerical values are listed in Table I. Most of the values given are representative of human heart data or animal muscle data, the primary exception being the maximum isometric muscle stress. The experimentally determined values for animal heart (papillary) muscle range from 2 to 10 g/mm^2, while a value of 16.5 g/mm^2 was found to be necessary for the heart model simulation of a normal LV. The discrepancy between the experimental values and the value required by the model may reflect a basic difference between heart wall muscle and papillary muscle. Since the papillary muscle does not act to eject blood but only to maintain closure of the mitral valve, it is not unlikely that it is weaker than wall muscle. The maximum muscle stress required by this model is in agreement with values reported by other investigators using other mathematical models of human cardiac stress.

SUMMARY

A detailed review of the development of a mathematical simulation of human LV function has been presented. Results from the simulation of human experimental data were presented showing the accuracy of the simulation and illustrating the prediction of the time variation of several variables which are as yet unmeasurable by experiment. The LV model not only incorporates muscle mechanics and thermodynamics on the ultrastructural level, but a simplified, rational fiber structure is used for the first time in a dynamic LV model. The computed values of measurable quantities agree well with experimental data presented in the open literature. A comparison of these computed values from this model and a previous model shows an improvement in the ability of heart models to predict physiologically realistic results.

Although many of the computed quantities in the model, such as fiber stress and CE length, cannot be measured, it is of interest that the computed values agree with

what is reasonably expected in the heart. The geometry of the heart requires that the endocardial fibers shorten more than epicardial fibers. Since the duration of contraction is the same for both, the epicardial fibers have a lower velocity than the endocardial ones. The model does reflect these rather obvious expected variations. Further, if an inverse force velocity relationship applies to cardiac muscle then the pattern of diminishing stress through the heart wall must result.

The heart model in its present form represents an initial approach to the problem of simulating cardiac function in detail. It is recognized that improvements in LV shape, fiber orientation, and muscle mechanics are possible and are underway. In particular, the assumption of spherical geometry is unrealistic from a physiological viewpoint and does introduce potentially significant errors into the stress distribution. For that reason the adoption of an elliptical geometry for the ventricle is one of the most important modifications being made in the model presented here. Nevertheless, the present model is believed to be unique in its detail and accuracy of simulation and of potentially significant clinical value.

This research was supported by the Columbus Laboratories of Battelle Memorial Institute.

Received for publication 11 April 1972.

REFERENCES

1. MASON, D. T., J. F. SPANN, JR., and R. ZELIS. 1970. *Am. J. Cardiol.* **26**:248.
2. SONNENBLICK, E. H., W. W. PARMLEY, and C. W. URSCHELL. 1969. *Am. J. Cardiol.* **23**:488.
3. BRAUNWALD, E., J. ROSS, JR., and E. H. SONNENBLICK. 1967. *New Engl. J. Med.* **277**:794, 853, 910, 962, 1012.
4. MASON, D. T. 1967. *Am. J. Cardiol.* **23**:516.
5. WEISSLER, A. M., W. S. HARRIS, and C. D. SCHOENFELD. 1969. *Am. J. Cardiol.* **23**:577.
6. ARONOW, W. S. 1969. *Am. J. Cardiol.* **26**:238.
7. POLLACK, G. H. 1970. *Circ. Res.* **26**:111.
8. SONNENBLICK, E. H. 1970. *Circ. Res.* **26**:479.
9. BENEKEN, J. E. W., and B. DEWIT. 1967. *In* Physical Bases of Circulatory Transport. E. B. Reeve and A. C. Guyton, editors. W. B. Saunders Company, Philadelphia. **1**:1.
10. NOORDERGRAAF, A. 1969. *In* Biological Engineering. H. P. Schwan, editor. McGraw-Hill Book Company, New York. **5**:391.
11. JAGER, G. N., N. WESTERHOF, and A. NOORDERGRAAF. 1965. *Circ. Res.* **16**:121.
12. SNYDER, M. F., V. C. RIDEOUT, and R. J. HILLESTAD. 1968. *J. Biomech.* **1**:341.
13. DICK, D. E., and V. C. RIDEOUT. 1965. Proceedings of the 18th Annual Conference on Engineering in Medicine and Biology, Philadelphia.
14. SNYDER, M. F., and V. C. RIDEOUT. 1969. *IEEE (Inst. Electr. Electron. Eng.) Trans. Bio-Med. Eng.* **4**:325.
15. JOHNSON, E. A., and P. W. KUOHUNG. 1968. *Math. Biosci.* **3**:65.
16. CARDUS, D., and R. K. ZEIGLER. 1968. *Comput. Biomed. Res.* **1**:508.
17. PICKERING, W. D., P. N. NIKIFORUK, and J. E. MERRIMAN. 1969. *Med. Biol. Eng.* **7**:401.
18. ROBINSON, D. A. 1965. *Circ. Res.* **17**:202.
19. BURTON, A. C. 1965. Physiology and Biophysics of the Circulation. Year Book Medical Publishers, Inc., Chicago.
20. RUSHMER, R. F. 1970. Cardiovascular Dynamics. W. B. Saunders Company, Philadelphia. 3rd Edition. **1**:1.
21. HILL, A. V. 1938. *Proc. R. Soc. Lond. B Biol. Sci.* **126**:136.

22. HUXLEY, A. F. 1957. *In* Progress in Biophysics. J. A. V. Butler and B. Katz, editors. Pergamon Press, New York. **7**:255.
23. CAPLAN, S. R. 1966. *J. Theor. Biol.* **11**:63.
24. WILKIE, D. R., and R. C. WOLEDGE. 1967. *Proc. R. Soc. Lond. B Biol. Sci.* **169**:17.
25. BORNHORST, W. J., and J. E. MINARDI. 1969. *Biophys. J.* **9**:654.
26. BORNHORST, W. J. and J. E. MINARDI. 1970. *Biophys. J.* **10**:137.
27. BORNHORST, W. J., and J. E. MINARDI. 1970. *Biophys. J.* **10**:155.
28. GORDON, A. M., A. F. HUXLEY, and F. J. JULIAN. 1966. *J. Physiol.* (*Lond.*). **184**:170.
29. PARMLEY, W. W., and E. H. SONNENBLICK. 1967. *Circ. Res.* **20**:112.
30. Fung, Y. C. 1971. *J. Biomech.* **4**:289.
31. SIEGEL, W. H., and E. H. SONNENBLICK. 1963. *Circ. Res.* **12**:600.
32. SPOTNITZ, H. M., E. H. SONNENBLICK, and D. SPIRO. 1966. *Circ. Res.* **18**:49.
33. STREETER, D. D., JR., and D. L. BASSETT. 1966. *Anat. Rec.* **155**:503.
34. STREETER,D.D., JR., H. M. SPOTNITZ, D. J. PATEL, J. ROSS, JR., and E. H. SONNENBLICK. 1969. *Circ. Res.* **24**:339.
35. BURNS, W. H., and N. J. GRIFFITH. 1968. American Society of Mechanical Engineers no. 68-WA/ENER-13.
36. MOUNTCASTLE, V. B. 1968. Medical Physiology. The C. V. Mosby Company, St. Louis, Mo. 12th edition.
37. STREETER, D. D., JR., R. N. VALSHNAV, D. J. PATEL, H. M. SPOTNITZ, J. ROSS, JR., and E. H. SONNENBLICK. 1970. *Biophys. J.* **10**:345.
38. RUSSELL, R. O., C. M. PORTER, M. FRIMMER, and H. T. DODGE. 1971. *Am. Heart J.* **81**:799.